Adaptive Cascade Control of a Brake-By-Wire Actuator for Sport Motorcycles

Fabio Todeschini, Matteo Corno, Giulio Panzani, Simone Fiorenti, and Sergio M. Savaresi

I. Introduction and Motivation

In the last years, the automotive industry has looked for innovative brake-by-wire (BBW) solutions: This to increase the vehicle performance and safety. The possibility of smoothly and precisely applying a desired braking torque is at the basis of many vehicle dynamics control [1]–[7] and autonomous vehicles.

Different technological solutions have been proposed: the electrohydraulic one (EHB) is based on a hydraulic system, which is activated by an electric motor or pump controlled by an electronic unit [8]–[11]. The electromechanical brake (EMB) solution does not have the hydraulic part but there is an electric motor as actuator that provides the braking torque [12]–[14]. A particular EMB technology is known as *wedge brake*, where an electric motor controls the force on a wedge that pushes backward and forward the braking pads [15], [16]. In this paper, we consider a modified EHB solution first presented in [17]–[19]: an electromechanical actuator that pushes backward and forward the piston of a master cylinder connected to a traditional hydraulic brake. Compared to well-known EMB and EHB solutions, this one has the advantage to keep the usual hydraulic layout adding just the actuator. This saves weight, space, and cost. With this architecture, the actuator control problem consists in tracking a desired pressure reference. As shown later on, the control problem is made nontrivial by the nonlinearities of the system (friction, presence of the brake fluid reservoir, temperature variation, and oil compressibility) and by the very demanding performance specifications. The BBW system is designed for racing application, where it is indispensable to have bandwidth greater than 10 Hz, no overshoot and good robustness. For technological constraints, at the end of the braking event the master cylinder piston must retract before the brake reservoir inlet so that a proper fluid compensation can be achieved. As discussed in the sequel, this introduces a nonlinearity in the system to be controlled. Furthermore, the control law must be robust to the so-called *knock-off*. In racing applications, at times, the brake disk pushes back the pads at the end of the braking event. This leads to a variation in the position-pressure characteristic: during the following braking action, the master cylinder must move further than in the previous one. Then, after this anomalous braking event, the system returns to the normal behavior. This happens in traditional brake too. Professional pilots feel the *knock-off* from the return force on the lever, and once detected, they compensate it by pressing the brake lever more.

To the best of the authors' knowledge, there are no other example of control of EHB for motorcycles, except for authors' previous works. The authors in [19] showed the need of a more complex controller than a simple linear pressure controller: the closed-loop response with a direct pressure controller shows a big overshoot that prevents its usage in this application. In [17], the issue is addressed by simply avoiding to completely retract the piston. In this way, a good pressure tracking performance is achieved at the cost of the risk of not compensating fluid volume changes. Moreover, a small pressure is always applied to the brake pads: This causes a loss of energy and a continuous brake pad wear. In [18] and [19], a hybrid position—pressure switching control strategy has been proposed, in this way, through the position control, it is possible to compensate the fluid volume variation at the end of each braking event. The main problem of such an architecture is that in the first phase of the braking action—when the position controller is enabled—the pressure is not directly controlled. So, if there is a small error in the identified position–pressure map, the control performances are affected. Moreover, the architecture proposed in [18] and [19] suffers from robustness issues.

In this paper, the aforementioned shortcomings are addressed by an adaptive cascade control architecture, which guarantees the required performance and improves robustness with respect to external disturbances. Also, experimental results that prove the effectiveness of the control law are presented.

Manuscript received October 18, 2013; revised June 25, 2014; accepted July 7, 2014. Recommended by Technical Editor M. Iwasaki.

F. Todeschini, M. Corno, S. Fiorenti, and S. M. Savaresi are with the Dipartimento di Elettronica, Informazione e Bioingegneria, Politecnico di Milano, 20133 Milan, Italy (e-mail: fabio.todeschini@polimi.it; corno@elet.polimi.it; fiorenti@elet.polimi.it; savaresi@elet.polimi.it).

G. Panzani is with the Institute for Dynamic Systems and Control, ETH Zurich, 8092 Zurich, Switzerland (e-mail: gpanzani@ethz.ch).

Color versions of one or more of the figures in this paper are available online.

TABLE I
ELECTROMECHANICAL BBW ACTUATOR (DC MOTOR, TRANSMISSION AND MECHANICAL FRAME) GENERAL SPECIFICATIONS

Weight	950	g
Height	42	mm
Length	105	mm
Width	75	mm
Motor Power	200	W

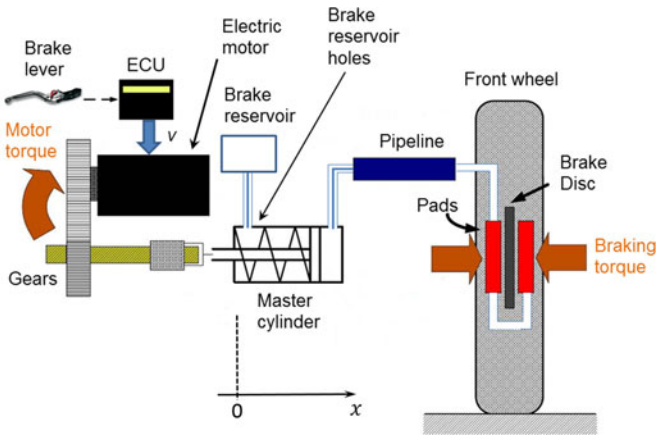

Fig. 1. Schematic representation of the BBW system.

This paper is structured as follow: in Section II, there is a brief description of the system, in Section III, a control-oriented model is derived; analyzing it, a cascade position–pressure control architecture is proposed. In Section IV, a gray-box identification method is adopted to derive the system model that is then used to tune the pressure and position loops. Since the pressure control law is nonlinear and time varying, a stability analysis is performed (see Section V). Finally, Section VI shows experimental results and Section VII the conclusions.

II. SYSTEM DESCRIPTION

The BBW system here considered is composed of an electromechanical actuator mechanically connected to a traditional hydraulic brake; in Table I, the BBW actuator general specifications are listed. Fig. 1 shows a schematic representation of the system.

The main components are as follows.

1) *Brake lever:* The pilot generates the reference pressure through it.
2) *BBW actuator:* An electronic control unit controls a dc motor that moves the master cylinder forward and backward through a mechanical transmission. In particular, the electronic board has a power bridge able to apply a voltage v on the motor clamps. The motor control is done through a current loop with a $100-$ Hz bandwidth. The motor spinning is transformed into a linear movement by means of a mechanical transmission. The actuator has a return spring that pushes the master cylinder backwards when no force is applied.
3) *Hydraulic brake:* The master cylinder piston movement varies the pressure in the hydraulic pump, that, through the pipe, is transmitted to the brake caliper. An important part of this subsystem is the brake reservoir: at the end of each braking event, the master cylinder piston must retract before the brake reservoir holes. In this way, the system compensates fluid volume variation due to temperature and brake pad wear.
4) *Mechanical brake:* Depending on the pressure in the brake caliper, the brake pads push against the brake disk, generating the braking torque.

The aim of this study is to find a control law that tracks the desired pressure. Available measures are the linear position of the master cylinder piston (x), the pressure in the hydraulic part (p), and the motor current (I). By convention, $x = 0$ mm is when the master cylinder is completed retracted and as it moves forward, x increases.

The pressure control law is implemented on a real-time microprocessor with a 200-Hz sample frequency.

III. SYSTEM MODELING

Starting from the physical elements composing the BBW actuator, the complete model can be derived [17], [18]. Instead, in this study, a control-oriented model is presented, its linearization in different working points gives considerations that lead to the control architecture here presented.

Consider the following assumptions:

1) thanks to the presence of the motor current loop, which is an order of magnitude faster than the pressure dynamics, the electrical dynamics can be discarded. Therefore, the current is considered as the control variable;
2) the pressure in the master cylinder and the pressure in the brake caliper are the same. In other words, we neglect the pressure wave propagation dynamics (the first resonance mode is usually around hundreds of hertz);
3) the amount of fluid volume in the system is not influenced by master cylinder position changes;
4) the static Coulomb friction is disregarded. This can be done if a dithering signal is applied to the control variable ([18]–[20]) or if a suitable friction compensation technique is applied ([21]–[23]). Under this assumption, we consider just the viscous friction contribution.

It is then possible to derive a second-order control-oriented model.

$$M_{\mathrm{eq}}\ddot{x} + K_{\mathrm{damp}}\dot{x} + K_{\mathrm{spring}}x + p(x)A_{\mathrm{mc}} = iQ_{\mathrm{eq}} \qquad (1)$$

where

1) $M_{\mathrm{eq}}\ddot{x}$ represents the mechanical inertial force and it can be computed as $M_{\mathrm{eq}} = M_{\mathrm{pist}} + J_{\mathrm{mot}}/K^2$, where M_{pist} is the master cylinder piston mass, J_{mot} is the motor moment of inertia, and K is the transmission ratio;
2) $K_{\mathrm{damp}}\dot{x}$ represents the damping force (due to viscous friction) and in general, it is unknown;
3) $K_{\mathrm{spring}}x$ represents the return spring force;
4) $p(x)A_{\mathrm{mc}}$ represents the return force due to the pressure in the master cylinder;

TABLE II
BBW COMPONENTS PHYSICAL PARAMETERS

M_{pist}	10^{-3}	kg
J_{mot}	$1.37\,10^{-5}$	$\mathrm{kg/m^2}$
A_{mc}	$1.13\,10^{-4}$	$\mathrm{m^2}$
K_T	0.0168	Nm/A
K	$0.3036\,10^{3}$	m/rad
K_{spring}	3000	N/m

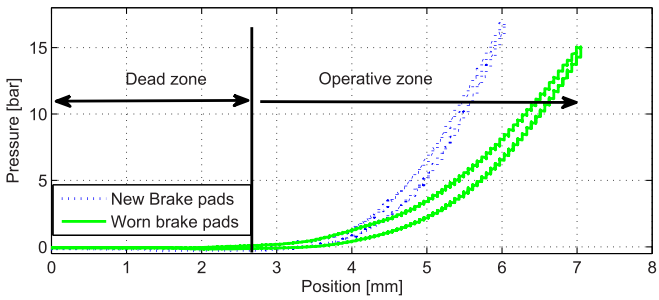

Fig. 2. Master cylinder position and pressure relationship with new and wore braking pads.

5) iQ_{eq} represents the equivalent force applied by the motor to the master cylinder piston and can be computed as K_T/K, where K_T is the motor torque constant.

The model parameters are listed Table II. Note that they can be found from the BBW physical components, the only unknown parameter is K_{damp}. In order to model the relationship between position and pressure, we exploit the quasi-static experimental response of the system when an increasing current ramp followed by a decreasing one is applied, depicted in Fig. 2 ($0\,A \rightarrow 10\,A$ in 30 s, then $10\,\mathrm{A} \rightarrow 0\,\mathrm{A}$ in 30 s). This is a nonlinear static map.

The position–pressure map can be divided in two different zones (see Fig. 2): in the dead zone, where the master cylinder is before the brake reservoir, the piston moves with no pressure variation. The dead zone is not affected by temperature and brake pad wear. The second part of the position–pressure curve is the operative zone; the master cylinder is after the brake reservoir and a position increment corresponds to a pressure increment. This part of the position–pressure curve is strongly affected by temperature and brake pads wear. Note that the position–pressure map depicted in Fig. 2 presents an hysteresis: The average curve is considered for modeling purpose. The position–pressure curve introduces a time varying nonlinearity in the model (1), as it changes with temperature and pads wear.

The linearized model allows for a quantification of the effect of the nonlinearity. Two different dynamics are analyzed: the current-to-position dynamics and the current-to-pressure one. Consider the linearized model

$$M_{\mathrm{eq}}\delta\ddot{x} + K_{\mathrm{damp}}\delta\dot{x} + K_{\mathrm{spring}}\delta x + A_{\mathrm{mc}}p^{'}(\bar{x})\delta x = \delta i Q_{\mathrm{eq}} \tag{2}$$

where

$$p^{'}(\bar{x}) = \left.\frac{\partial p(x)}{\partial x}\right|_{x=\bar{x}} \tag{3}$$

is the slope of the pressure–position map in the working point ($\bar{x}$). The transfer function between current and position is

$$G_x(s) = \frac{Q_{\mathrm{eq}}}{M_{\mathrm{eq}}s^2 + K_{\mathrm{damp}}s + A_{\mathrm{mc}}p^{'}(\bar{x})} \tag{4}$$

where K_{spring} has been considered negligible compared to $A_{\mathrm{mc}}p^{'}(\bar{x})$. From (4), it can be seen that:

1) the low-frequency gain is

$$\lim_{s\to 0} G_x(s) = \frac{Q_{\mathrm{eq}}}{A_{\mathrm{mc}}p^{'}(\bar{x})} \tag{5}$$

thus, it decreases as the working position increases.

2) the high-frequency gain is

$$\lim_{s\to \infty} G_x(s) = \frac{Q_{\mathrm{eq}}}{M_{\mathrm{eq}}s^2} \tag{6}$$

which is independent from the working point.

Also, by recalling the linearized link $\delta p = p^{'}(\bar{x})\delta x$, the transfer function between current and pressure can be derived.

$$G_p(s) = \frac{Q_{\mathrm{eq}}p^{'}(\bar{x})}{M_{\mathrm{eq}}s^2 + K_{\mathrm{damp}}s + A_{\mathrm{mc}}p^{'}(\bar{x})}. \tag{7}$$

Then, analyzing the obtained transfer function:

1) the low-frequency gain is

$$\lim_{s\to 0} G_p(s) = \frac{Q_{\mathrm{eq}}}{A_{\mathrm{mc}}} \tag{8}$$

therefore, it is independent from the working point.

2) the high-frequency gain is

$$\lim_{s\to 0} G_p(s) = \frac{Q_{\mathrm{eq}}p^{'}(\bar{x})}{M_{\mathrm{eq}}s^2} \tag{9}$$

which is working point dependent (its gain increases with it).

IV. CONTROL SYSTEM DESIGN

The transfer function analysis is the base to design the control architecture. The control architecture must deal with the presence of the dead zone (where a position controller is strictly needed), with different working points and with variations in the position–pressure map. Exploiting the fact that the position transfer functions are working point independent above a certain frequency, a specifically tuned linear position controller could make the closed loop robust with respect to the working point.

Furthermore, an outer pressure loop is needed: in fact, the position–pressure map is time varying due to temperature and pads wear; so adopting just a position control would not be precise in terms of pressure tracking. These considerations lead to a position–pressure cascade control architecture (see Fig. 3).

In the identification phase, we followed a gray-box identification approach. The control-oriented model derived in the previous section, beside being adopted to decide the control architecture, is exploited to determine the transfer functions order.

A. Position Loop

The aim of this section is to design a position loop able to track the reference with a closed-loop bandwidth around 50

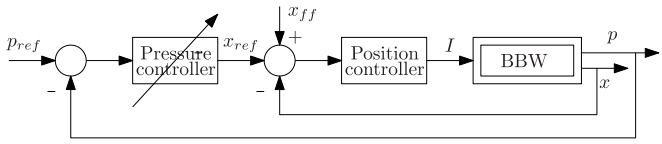

Fig. 3. Position–pressure cascade control.

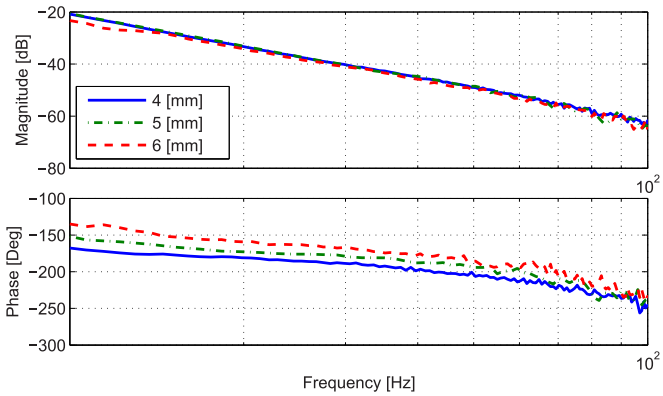

Fig. 4. Identified current → position transfer function in different working points.

Hz. The current-to-position model identification is performed around different working points ($\bar{x}$). The system is maintained around $\bar{x}$ by means of a 1-Hz bandwidth position controller. The excitation signal is a multifrequency sinusoidal current added into the loop as a load disturbance. The excitation signal frequency ranges from 10 to 200 Hz; this is consistent with the goal that we want to achieve.

Note that, in the identification process since the closed-loop bandwidth is low compared to the excitation signal frequency, the control action and the excitation signal are decoupled in frequency. The same process is done maintaining the system around different working points, for each of them, the input (current) and the output (the position) are collected. The frequency response around each working point can be derived (see Fig. 4) as the quotient of the cross power spectral density output ($T_{yx}(j\omega)$) and input ($T_{xx}(j\omega)$), i.e., the generic frequency response $G(j\omega)$ is computed as follows:

$$G(j\omega) = \frac{T_{yx}(j\omega)}{T_{xx}(j\omega)}. \tag{10}$$

Fig. 4 shows the identified frequency responses from 10 to 100 Hz in different working points, where their convergence after 10 Hz can be appreciated, this confirms the analysis of Section III. Note that from that analysis, the phase of the frequency response should be $-180°$. The loss of phase in the experimental frequency response around 10 Hz is determined by the low-frequency poles that the current-to-position transfer function have. The position of the two poles is influenced by the working point [see (4)]. Instead, the phase difference around 100 Hz is caused by the low energy that the output signal has at those frequencies.

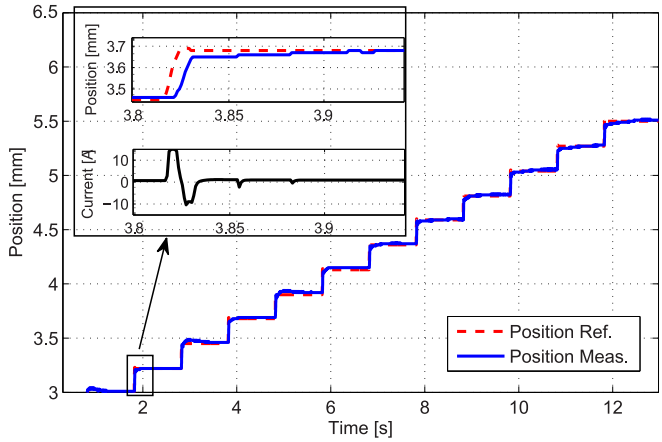

Fig. 5. Position loop validation.

The current-to-position identification confirms the analysis carried out in Section III, thus, designing a position controller with a bandwidth greater than 10 Hz and a wide phase margin, robustness with respect to the working point is guaranteed with a fixed structure linear controller. A PID controller is designed on the worst case scenario using classical loop shaping techniques to obtain a 50-Hz bandwidth with a phase margin $\phi_m = 85°$, Fig. 5 plots series of closed-loop position reference step adopting the designed controller. The experiment validates the robustness and performance of the control loop.

B. Pressure Loop

The final control objective is pressure tracking and since the position–pressure relationship has a hysteresis and it is time varying, a standalone position loop is not enough, a pressure loop is required. The pressure loop must deal with the position–pressure nonlinearity depicted in Fig. 2 and it has to provide the same tracking performance under every condition. Since in the dead zone the pressure growth is negligible, the pressure controller will be designed to work in the operative zone. To cope with the presence of the dead zone, however, a supervising finite-state machine is presented, that guarantees the proper controller working throughout the entire position–pressure map.

When designing the pressure controller in the cascade architecture, the control variable of interest is the reference position. The reference position → pressure transfer function is, therefore, identified. The identification scheme adopted exploits the position controller designed in the previous subsection: a multifrequency reference position is injected; note that its average value establishes the working point where the identification is performed. Collecting the system input (reference position), together with the output (the pressure), a transfer function in each working point can be computed from the input/output cross power spectral density (solid lines in Fig. 6).

Note that the static gain of the transfer function corresponds to the slope of the position–pressure map presented in Fig. 2. Moreover, the dynamic behavior is the same in every working point. The frequency response identified around 3.5 mm (solid

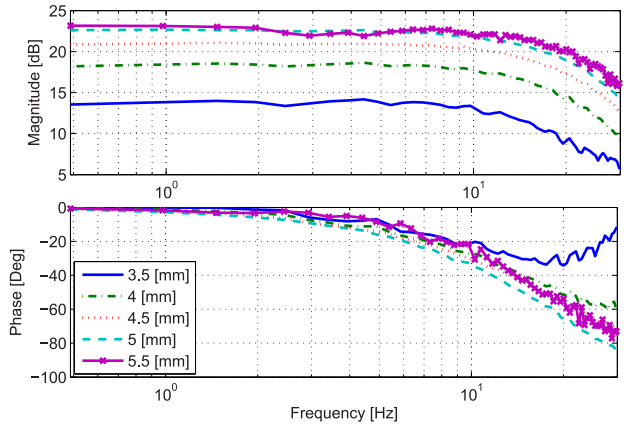

Fig. 6. Identified reference position → pressure transfer functions in different working points.

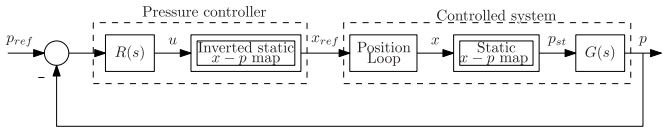

Fig. 7. Schematic representation of the pressure control problem.

line in Fig. 6) can be considered reliable up to 20 Hz; after that frequency, the system does not have enough excitation to collect consistent data.

For this, the position–pressure relationship is modeled as a Hammerstein system, i.e., with a cascade connection of a static nonlinearity block followed by a linear dynamic system [24].

The static nonlinearity is modeled by a second-order polynomial

$$p_{\mathrm{st}} = a(x - x_{dz})^2 + b(x - x_{dz}) \tag{11}$$

x_{dz} represents the position where the master cylinder piston completely overcomes the brake reservoir, so where the operative-zone starts (see Fig. 6). In (11), a gives the concavity of the curve, which is always positive.

The system dynamics (represented in Fig. 7 with $G(s)$) are modeled as a first-order system with unitary gain

$$G(s) = \frac{1}{T_i s + 1}. \tag{12}$$

Note that in the modeling section (see Section III) the position–pressure relationship was assumed to be static: the considerations done that brought to the choice of the proposed cascade architecture hold also if we consider the dynamics between them.

Assuming that the position loop is much faster than the pressure dynamics and that a and b are constant, the position–pressure relationship can be exploited and inverted in the controller. Referring to Fig. 7, applying the following static map between u and x_{ref}

$$x_{\mathrm{ref}} = \frac{-b_* + \sqrt{b_*^2 + 4a_* u}}{2a_*} \tag{13}$$

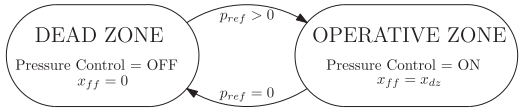

Fig. 8. Finite-state machine that supervises the cascade control architecture.

and assuming that the controller parameters are the same of the plant ones ($a_* = a$ and $b_* = b$), the series of the two nonlinearity becomes a unitary block, i.e., $u = p_{\mathrm{st}}$. So, the closed loop becomes linear and the design of $R(s)$ on $G(s)$ is trivial. In particular, adopting a simple PI controller with a zero at the same frequency of the system pole, the loop transfer function becomes

$$L(s) = R(s)G(s) = \frac{k_p}{s} \tag{14}$$

where k_p determines the closed-loop bandwidth. In this ideal case, the loop transfer function is an integrator and the closed-loop performances are pressure invariant. The design of $R(s)$ is done in order to achieve a 15-Hz bandwidth (phase margin $\phi_m = 90°$ and gain margin $\mu_g = \infty$). In Section V, the stability of the pressure loop is discussed when $a \neq a_*$ and $b \neq b_*$.

With the aim of extending the control architecture (see Fig. 3) to the dead zone, the finite-state machine shown in Fig. 8 is introduced. Its main goal is to enable the pressure control only when the system is in the operative zone, otherwise no pressure tracking is necessary, therefore, the position loop suffices. When there is no pressure request ($p_{\mathrm{ref}} = 0$), the `DEAD ZONE` state is enabled, so the pressure controller is switched OFF and the position reference is null. In this state, the position *feed-forward* (x_{ff}) is null too. Then, when there is pressure request ($p_{\mathrm{ref}} > 0$), the system goes in the `OPERATIVE ZONE` state, where the pressure controller is enabled and the position reference *feed-forward* is set in order to overcome the dead zone with the position loop response time ($x_{\mathrm{ff}} = x_{\mathrm{dz}}$).

C. Adaptation Mechanism

Until now, we considered the static nonlinear gain between position and pressure as constant; in fact it varies with temperature and brake pad wear. This static map can be recursively estimated. Recalling (11)

$$\hat{p}_{\mathrm{st}}(t) = \phi_E(t)^T \cdot \hat{\theta} = \left[\, x(t) - x_{\mathrm{dz}} \;\; (x(t) - x_{\mathrm{dz}})^2 \,\right] \cdot \begin{bmatrix} b^* \\ a^* \end{bmatrix} \tag{15}$$

the estimation error can be computed as

$$\epsilon(t) = p_{\mathrm{st}}(t) - \hat{p}_{\mathrm{st}}(t). \tag{16}$$

A recursive least-square algorithm with a fixed forgetting factor (μ) has been implemented as

$$\begin{cases} \hat{\theta}_t = \hat{\theta}_{t-1} + K(t)\epsilon(t) \\ K(t) = V(t)\phi_E(t) \\ V(t) = \frac{1}{\mu}\left(V(t-1) - \beta_{t-1}^{-1} V(t-1)\phi_E(t) \right. \\ \qquad \left. \cdot \phi_E(t)^T V(t-1)\right) \\ \beta_{t-1} = \mu + \phi_E(t)^T V(t-1)\phi_E(t). \end{cases} \tag{17}$$

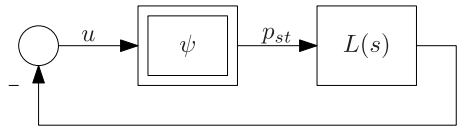

Fig. 9. Pressure loop seen as a Lur'e system: A nonlinear block with a linear one.

The estimation process is enabled by the finite-state machine in Fig. 8. The forgetting factor μ needs to be chosen so that the estimation algorithm tracks the variation due to temperature and pad wear; if too high, a forgetting factor is employed, the controller will not adapt to variation; if too low, a forgetting factor affects the reliability and could compromise the stability of the closed loop. Ideally, the estimation algorithm weights data from two or three braking events. This is obtained with $\mu = 0.995$.

V. Stability Analysis

The pressure controller has been tuned under the assumption of perfect compensation of the nonlinearity. In this section, the controlled system stability in the case of nonperfect compensation is analyzed. The nonlinearity estimation error is modeled as a multiplicative uncertainty

$$\begin{cases} a_* = \ k_1 a \\ b_* = \ k_2 b \end{cases} \tag{18}$$

where k_1 and k_2 represent the discrepancy between the real parameters and the ones used in the controller. The estimator dynamics is decoupled from the closed loop one, thus, we can treat k_1 and k_2 as unknown but constant. The pressure controller has a dynamic part that cancels the system pole; also this simplification may not be perfect

$$T_{i*} = \ k_3 T_i \tag{19}$$

so k_3 represents the pole estimation error. We can reasonably assume that the sign of the parameters is correctly identified; in other words, $k_i > 0$. As previously done in the pressure controller design phase, assuming that the position loop is fast enough compared to the pressure one, it is considered as ideal.

Proposition 1: The closed-loop system depicted in Fig. 7, composed of the position-controlled BBW system (see Section A) and the nonlinear characteristic (13) compensating the PI control action, is globally asymptotically stable for all $k_i \in [0.25, 4]$.

Proof: The block diagram depicted in Fig. 7 is manipulated, obtaining a Lur'e system as shown in Fig. 9.

Therefore, the closed-loop system can be seen as a series connection between a dynamic part (the controller and the plant)

$$L(s) = R(s)G(s) = \frac{k_p(1 + T_{i*}s)}{s(1 + T_i s)} \tag{20}$$

and a static part

$$\psi(u, k_1, k_2) = u\tfrac{1}{k_1} + \tfrac{k_2 b^2 (k_1 - k_2)}{2ak_1^2} \left(\sqrt{1 + \tfrac{4k_1 au}{k_2^2 b^2}} - 1 \right) \tag{21}$$

which describes the relationship between u and p_{st}. Equation (21) is composed of a linear term and a nonlinear one.

The closed-loop stability depends on $\psi(u, k_1, k_2)$ and on k_3. In particular:

1) if the position–pressure map is perfectly known ($k_1 = k_2 = 1$), then $\psi(u, k_1, k_2) = u$. This is the ideal case discussed in Section IV-B;
2) if $k_1 = k_2 \neq 1$, then $p_{\rm st} = \frac{u}{k_1}$. The loop transfer function is linear and it is equal to $\frac{L(s)}{k_1}$. The stability of such a system depends on the pole identification precision (k_3) and can be studied adopting the Bode's method (i.e., phase and gain margin);
3) if $k_1 \neq k_2 \neq 1$, the relationship between u and $p_{\rm st}$ is described by (21). In this case, the stability proof is based on the circle criterion [25], [26]. First of all, the nonlinearity is studied in order to prove that it is a sectorial nonlinearity, i.e., that $\underline{\psi} u < \psi(u, k_1, k_2) < \overline{\psi} u$. Rewriting (21) as

$$\psi(u, k_1, k_2) = u\frac{1}{k_1} + A\left(\sqrt{1 + Bu} - 1\right) \tag{22}$$

where $A = \frac{k_2 b^2 (k_1 - k_2)}{2ak_1^2}$, $B = \frac{4k_1 a}{k_2^2 b^2}$ and differentiating it with respect to u

$$\frac{\partial \psi}{\partial u} = \frac{1}{k_1} + \frac{AB}{2\sqrt{1 + Bu}} \tag{23}$$

we can note that:

a) since a is always positive, then $B > 0$;
b) $\psi|_{u=0} = 0$;
c) if $k_1 > k_2$ ($A > 0$), then $\frac{\partial \psi}{\partial u}$ is decreasing, otherwise is increasing as u increases;
d) $\frac{\partial \psi}{\partial u}|_{u=0} = \frac{1}{k_1} + \frac{AB}{2}$;
e) $\lim_{u \to \infty} \frac{\partial \psi}{\partial u} = \frac{1}{k_1} > 0$.

$\psi(u, k_1, k_2)$ is monotonically increasing, and since $\psi(0, k_1, k_2) = 0$ for every k_1, k_2

$$\psi(u, k_1, k_2) \in [0, +\infty). \tag{24}$$

Furthermore, an upper ($\overline{\psi} u$) and a lower limiting functions ($\underline{\psi} u$) can be found. If $k_1 > k_2$, considering the following limiting functions:

$$\begin{aligned} \overline{\psi} u &= \frac{u}{k_1} + \frac{ABu}{2} \\ \underline{\psi} u &= \frac{u}{k_1} \end{aligned} \tag{25}$$

then

$$\begin{cases} u\frac{1}{k_1} + A\left(\sqrt{1 + Bu} - 1\right) < \frac{u}{k_1} + \frac{ABu}{2} \\ u\frac{1}{k_1} + A\left(\sqrt{1 + Bu} - 1\right) > \frac{u}{k_1} \end{cases} \tag{26}$$

which yields to

$$\begin{cases} \frac{(Bu)^2}{4} > 0 \quad \forall u \\ A\left(\sqrt{1 + Bu} - 1\right) > 0 \quad \forall u. \end{cases} \tag{27}$$

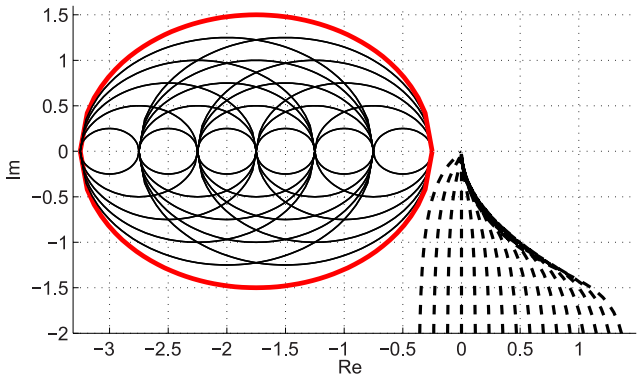

Fig. 10. Graphical proof of the validity of the circle theorem: L(s) Nyquist plot varying k_3 (dotted lines) and circles passing through $-1/\overline{\psi}$ and $-1/\underline{\psi}$ varying k_1 and k_2 (solid lines).

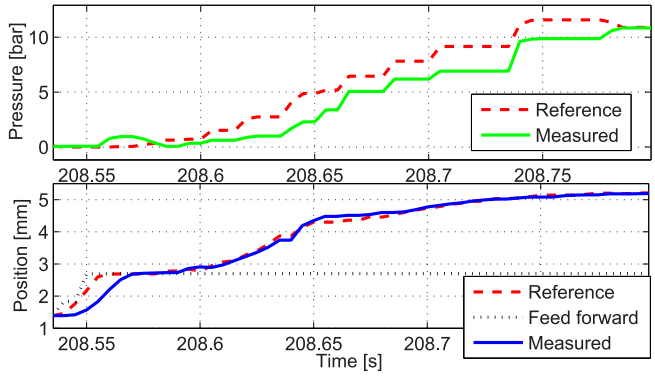

Fig. 11. Experimental results obtained during tests on a real circuit—zoom of the first part of a sharp braking event.

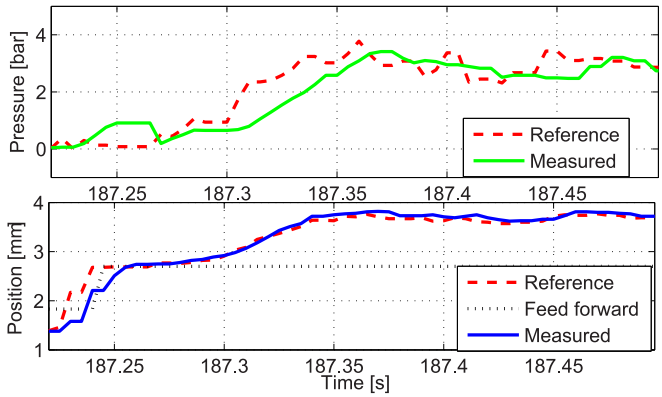

Fig. 12. Experimental results obtained during tests on a real circuit—zoom of the first part of a fine braking modulation.

Otherwise, if $k_1 < k_2$ and considering the following limiting functions

$$\begin{aligned} \overline{\psi}u &= \frac{u}{k_1} \\ \underline{\psi}u &= \frac{u}{k_1} + \frac{ABu}{2} \end{aligned} \tag{28}$$

then

$$\begin{cases} u\frac{1}{k_1} + A\left(\sqrt{1+Bu}-1\right) > \frac{u}{k_1} + \frac{ABu}{2} \\ u\frac{1}{k_1} + A\left(\sqrt{1+Bu}-1\right) < \frac{u}{k_1} \end{cases} \tag{29}$$

which yields to

$$\begin{cases} \frac{(Bu)^2}{4} > 0 \quad \forall u \\ A\left(\sqrt{1+Bu}-1\right) < 0 \quad \forall u. \end{cases} \tag{30}$$

Therefore. the nonlinearity is sectorial.

Exploiting the circle criterion, if the Nyquist diagram of $L(s)$ does not enter in the circle that passes through $-\frac{1}{\overline{\psi}}$ and through $-\frac{1}{\underline{\psi}}$, the closed-loop system is exponential globally stable. The method can be used to numerically check the robust stability of the control system. Fig. 10 is a graphical verification of the hypothesis of the circle theorem: the dotted lines are the $L(s)$ Nyquist plot varying k_3 so the loop transfer function varying the position of the dynamic part of the Hammerstein system (T_i in (12)). The solid lines are the circles passing through $-1/\overline{\psi}$ and $-1/\underline{\psi}$ varying k_1 and k_2. The results shown in Fig. 10 are obtained considering parameters variations as stated in proposition 1 ($k_i \in [0.25, 4]$).

The system is thus able in the face of a rather large uncertainty in the estimation.

VI. Experimental Results

In this section, the experimental results are presented: first the tracking performances are shown, then the effectiveness of the adaptation algorithm is validated.

A professional rider tested the BBW system on a racing circuit. He rode two identical high-performance motorbikes, one equipped with the BBW on the front wheel, the other one with standard brakes. From the experimental tests, it turned out that the most critical part of the braking action is the first part, where the controller must be fast enough in order to cross the dead zone, and then, track the pressure reference without exhibiting a delay. Furthermore, if the pressure loop is tuned with a bandwidth lower than 10 Hz, the driver can feel a delay in the front braking system. Also, if an overshoot greater than 25% is present the rider perceives it as a nonlinear braking response.

Fig. 11 shows the first part of a sharp braking action at the end of a straight when the main goal of the pilot is to decelerate the vehicle in the shortest time; while Fig. 12 shows a fine braking pressure modulation that typically happens during a curve. At the beginning of both braking events, the pressure loop is disabled and when the pressure reference becomes greater than zero, the position feed-forward term becomes x_{dz} so that the master cylinder overcomes the dead zone with a speed related to the position loop bandwidth. Then, once the dead zone is overcome, the pressure loop is enabled and the BBW system tracks the pressure reference. Note that, when the master cylinder piston quickly overcomes the dead zone a small pressure overshoot happens. This is due to the fast master cylinder movement in the dead zone. Experimental tests showed that the rider

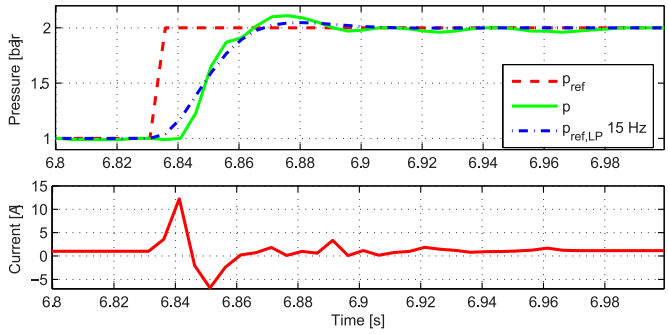

Fig. 13. Pressure reference step response.

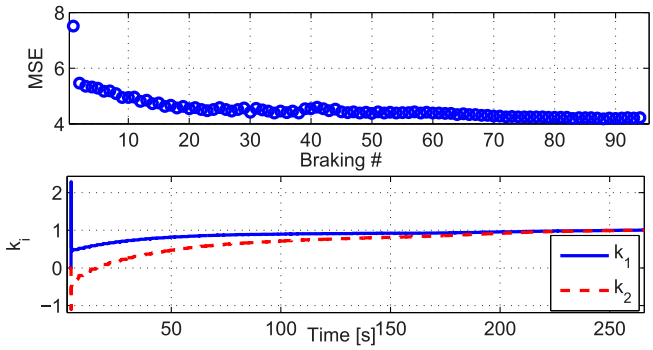

Fig. 14. Pressure MSE and coefficient estimation errors during braking events starting from a wrong initial conditions.

does not perceive the small overshoot at the beginning of the braking event.

In order to precisely evaluate the pressure closed-loop bandwidth, a step reference variation test is performed (see Fig. 13). On the top, subplot is superimposed the ideal pressure response, i.e., the pressure reference filtered with a 15-Hz low-pass filter. Note that the pressure closed loop has the expected bandwidth and that the current in this test does not saturate. For wider steps, the current saturation could slow down the pressure response.

The required closed-loop specifications are met: the pressure tracks the reference with a 15-Hz bandwidth, without overshoot and with delays shorter than the ones perceivable by a professional rider.

The final analysis validates the effectiveness of the adaptation algorithm. Starting from wrong initial parameters value estimation, the pressure mean square error (MSE) is analyzed as

$$\mathrm{MSE} = \sum_{t=1}^{t_{\mathrm{end}}} \frac{(p_{\mathrm{ref}}(t) - p(t))^2}{N} \tag{31}$$

where $p_{\mathrm{ref}}(t)$ and $p(t)$ represent the reference pressure and the measured pressure at the time t in the braking event considered. N is the number of samples collected between t and t_{end}. Fig. 14 shows that the adaptation algorithm updates the parameter values until k_1 and k_2 reach the right values. It can be appreciated how the MSE decreases as the estimated parameters converge to the real ones. This proves the effectiveness of adopting an adaptive control system.

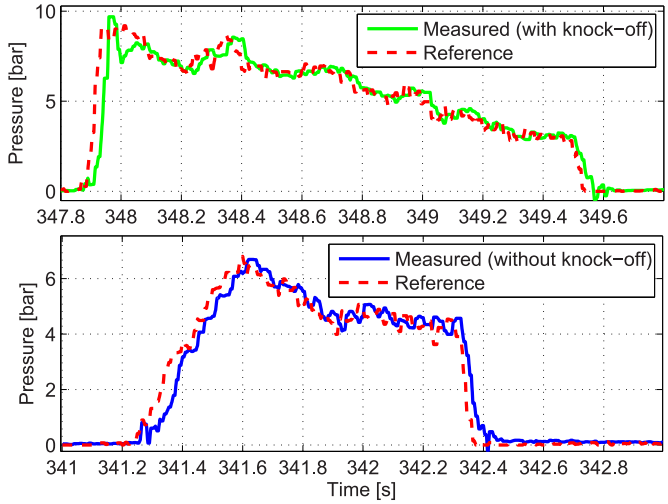

Fig. 15. Experimental pressure tracking when the *knock-off* causes a position–pressure curve variation (top plot) and in a nominal condition (bottom plot).

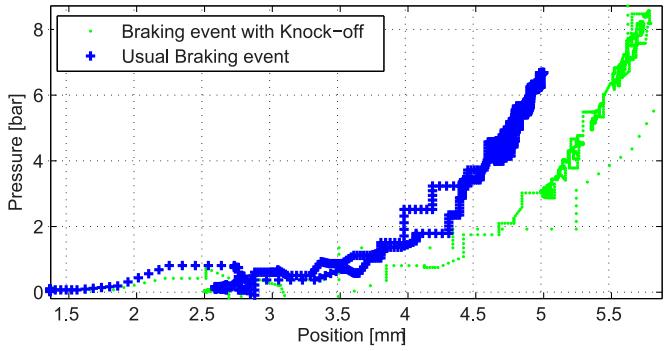

Fig. 16. Experimental position–pressure curve changing in the presence of the *knock-off*.

Furthermore, note that, since k_1 and k_2 were initialized with a considerable error to test the closed-loop robustness, they reach negative values. This means that the stability analysis is conducted under conservative hypotheses: in fact the closed-loop system remains stable even if k_1 and k_2 are out of the specified bounds. Initializing the estimation algorithm with more realistic values, k_1 and k_2 remains positive. Also, note that the estimator dynamic is decoupled from the pressure one.

The control architecture has been tested also in the presence of the *knock-off*, i.e., when a position–pressure curve modification happens from one braking event to another: the pressure tracking in the presence of the *knock-off* is shown in Fig. 15, while Fig. 16 shows the variation of the position–pressure in the same two braking events. The control architecture shows a good robustness with respect to position pressure changing. This is not surprising, when *knock-off* happens, it causes a sudden variation of a and b; in Section V, we proved that the system remains globally asymptotically stable even in the presence of parameter estimation errors.

VII. Conclusion

In this paper, the control of a novel BBW actuator is presented; such actuator presents nonlinear and time variant characteristics. The control architecture chosen derives from the analysis of the control-oriented model. In particular, the transfer function between current and position exhibits an important propriety: above a certain frequency, the system is insensitive to the working point. Exploiting this peculiarity, a cascade control is adopted: the inner loop is a position one, the outer loop a pressure one. Model identification procedure and controller design are presented for both loops. The pressure controller aims to invert the intrinsic nonlinear position–pressure relationship. Since this nonlinear relationship is influenced by temperature and brake pad wear, an estimation algorithm has been introduced. The complete control architecture is thus a cascade control with a nonlinear and adaptive pressure controller. Moreover, since the pressure controller bases the control law on the estimation of the plant parameters, an analytical stability analysis has been done. This study highlighted that the closed loop remain stable, even if the estimated parameters have relevant differences from the real ones. This study can be interpreted as a robustness proof: assuming that the position–pressure relationship is estimated correctly from (17), when a *knock-off* phenomenon happens, it is equivalent to a position–pressure curve instantaneous dilatation on the position axis. As the stability proof states, the closed-loop algorithm is able to handle parameters variation in this range: $k_i \in [0.25, 4]$.

In conclusion, the main improvements of the adaptive nonlinear cascade architecture are:

1) good robustness with respect to *knock-off*, i.e., with respect to sudden position–pressure changing. The stability analysis proves it analytically;
2) pressure tracking in every part of the braking event, even in the first part;
3) closed-loop bandwidth of 15 Hz.

References

[1] S. Anwar, "Generalized predictive control of yaw dynamics of a hybrid brake-by-wire equipped vehicle," *Mechatronics*, vol. 15, no. 9, pp. 1089–1108, 2005.

[2] M. Tanelli, A. Astolfi, and S. Savaresi, "Robust nonlinear output feedback control for brake by wire control systems," *Automatica*, vol. 44, no. 4, pp. 1078–1087, 2008.

[3] M. Tanelli, R. Sartori, and S. Savaresi, "Combining slip and deceleration control for brake-by-wire control systems: A sliding-mode approach." *Eur. J. Control*, vol. 13, no. 6, pp. 593–611, 2007.

[4] M. Corno, S. Savaresi, and G. Balas, "On linear-parameter-varying (LPV) slip-controller design for two-wheeled vehicles," *Int. J. Robust Nonlinear Control*, vol. 19, no. 12, pp. 1313–1336, 2009.

[5] M. Tanelli, M. Corno, I. Boniolo, and S. Savaresi, "Active braking control of two-wheeled vehicles on curves," *Int. J. Vehicle Auton. Syst.*, vol. 7, no. 3, pp. 243–269, 2009.

[6] T. Johansen, I. Petersen, J. Kalkkuhl, and J. Ludemann, "Gain-scheduled wheel slip control in automotive brake systems," *IEEE Trans. Control Syst. Technol.*, vol. 11, no. 6 pp. 799–811, Nov. 811.

[7] S. Savaresi, M. Tanelli, and C. Cantoni, "Mixed slip-deceleration control in automotive braking systems," *J. Dyn. Syst., Meas. Control*, vol. 129, pp. 20–31, 2007.

[8] D. Reuter, E. Lloyd, J. Zehnder, and J. Elliott, "Hydraulic design considerations for EHB systems," *presented at the SAE World Congr.*, MI, USA, 2003.

[9] N. D'alfio, A. Morgando, and A. Sorniotti, "Electro-hydraulic brake systems: Design and test through hardware-in-the-loop simulation," *Vehicle Syst. Dyn, Int. J. Vehicle Mech. Mobility*, vol. 44, no. 1, pp. 378–392, 2006.

[10] A. Sorniotti, and G. Repici, "Hardware in the loop with electro-hydraulic brake systems," *presented at the 9th WSEAS Int. Conf. on Systems*, Athens, Greece, 2005.

[11] V. Milanès, C. Gonzàlez, E. Naranjo, E. Onieva, and T. De Pedro, "Electro-hydraulic braking system for autonomous vehicles," *Int. J. Automotive Technol.*, vol. 11, no. 1, pp. 89–95, 2010.

[12] J. Kwak, B. Yao, and A. Bajaj, "Analytical model development and model reduction for electromechanical brake system," *presented at the Int. Mechanical Engineering Congr. and Exp.*, Anaheim, CA, USA, 2004.

[13] C. Line, "*Modelling and control of an automotive electromechanical brake*," Ph.D. Thesis, Univ. of Melbourne, Melbourne, Australia, 2007.

[14] C. Rossa, A. Jaegy, J. Lozada, and A. Micaelli, "Design considerations for magnetorheological brakes," *IEEE/ASME Trans. Mechatronics*, vol. 19, no. 5 pp. 1669–1680, Oct. 1680.

[15] H. Hartmann, M. Schautt, A. Pascucci, and B. Gombert, "ebrake®-the mechatronic wedge brake," in *Proc. SAE Conf. Proc. P*. SAE, 2002, pp. 15–20.

[16] R. Roberts, M. Schautt, H. Hartmann, and B. Gombert, "Modelling and validation of the mechatronic wedge brake," *SAE paper*, vol. 112, pp. 2376–2386, 2003.

[17] A. Dardanelli, G. Alli, and S. Savaresi, "Modeling and control of an electro-mechanical brake-by-wire actuator for a sport motorbike," *the 5th IFAC Symp. Mechatronic Sys.*, Cambridge, MA, 2010, pp. 524–531.

[18] G. Panzani, M. Corno, F. Todeschini, S. Fiorenti, and S. Savaresi, "Analysis and control of a brake by wire actuator for sport motorcycles," *presented at the 13th Mechatronics Forum Int. Conf.*, Linz, Austria, Sep. 17–19, 2012.

[19] F. Todeschini, M. Corno, G. Panzani, and S. M. Savaresi, "Adaptive position-pressure control of a brake by wire actuator for sport motorcycles," *Eur. J. Control*, vol. 20, no. 2, pp. 79–86, 2014.

[20] H. Olsson, K. Åström, C. Canudas de Wit, M. Gäfvert, and P. Lischinsky, "Friction models and friction compensation," *Eur. J. Control*, vol. 4, pp. 176–195, 1998.

[21] G. Panzani, M. Corno, and S. M. Savaresi, "On adaptive electronic throttle control for sport motorcycles," *Control Eng. Practice*, vol. 21, pp. 42–53, 2013.

[22] M. Michaux, A. Ferri, and K. Cunefare, "Effect of tangential dither signal on friction induced oscillations in an sdof model," *J. Comput. Nonlinear Dyn.*, vol. 2, pp. 201–210, 2007.

[23] J. L. Barreto, S. A. S. Conceicao, C. Dorea, L. Martinez, and E. de Pieri, "Design and implementation of model-predictive control with friction compensation on an omnidirectional mobile robot," *IEEE/ASME Trans. Mechatronics*, vol. 19, no. 2 pp. 467–476, Apr. 476.

[24] S. A. Billings, and S. Y. Fakhouri, "Identification of systems containing linear dynamic and static nonlinear elements," *Automatica*, vol. 18, no. 1 pp. 15–26, Jan. 26.

[25] G. Zames, "On the input-output stability of time-varying nonlinear feedback systems–Part ii, Conditions involving circles in the frequency plane and sector nonlinearities," *IEEE Trans. Automat. Control*, vol. 11, no. 3 pp. 465–476, Jul. 476.

[26] H. K. Khalil, *Nonlinear Systems*. Upper Saddle River, NJ, USA: Prentice Hall, 2002, vol. 3.